Discover Oncology

Research

Proteomics and succinylation modification characterization in clear cell renal cell carcinoma

Dong Yue[1] · **Miao Zheng**[2]

Received: 3 February 2025 / Accepted: 16 May 2025
Published online: 20 May 2025

Abstract
Clear cell renal cell carcinoma (ccRCC) represents the most lethal form of kidney cancer, with a significant number of patients experiencing tumor progression. Succinylation modification is a novel post-translational modification (PTM) that refers to modifying a protein with a succinyl group, which most frequently happens to lysine residues. Recent studies have revealed that abnormal succinylation, altered protein activity, dysfunctional roles in energy metabolism, and subsequent epigenetic modifications are linked to the onset and progression of conditions like inflammation, cancer, and other diseases. No studies have offered a comprehensive analysis of succinylation modification in ccRCC or clarified the mechanisms by which this modification operates within disease progression. In this study, we applied quantitative proteomics and succinylation modification omics to extensively examine the global proteome and succinylation modification changes in ccRCC tissues. Using high-throughput liquid chromatography-mass spectrometry, we identified 4801 lysine succinylation modification sites across 1274 proteins in ccRCC and adjacent non-cancerous tissues. Additionally, 434 succinylation sites within 328 proteins displayed significant differential modification in ccRCC (fold change (FC) > 1.5 or $p < 0.05$). Notably, the succinylated proteins were primarily associated with energy metabolism pathways, including fatty acid elongation, glyoxylate and dicarboxylate metabolism, the tricarboxylic acid cycle, and oxidative phosphorylation, and were predominantly located within the mitochondria. This study is the first to present a global proteomic profile and a detailed succinylation modification landscape in ccRCC. These findings introduce new potential approaches for treating ccRCC by reversing abnormal succinylation modifications.

Supplementary Information The online version contains supplementary material available at https://doi.org/10.1007/s12672-025-02737-3.

✉ Miao Zheng, yuedong2023@163.com; Dong Yue, yuedong2021@163.com | [1]Department of Urology, Affiliated Hospital of Jining Medical University, Jining, Shandong, China. [2]Department of Operating Room, Affiliated Hospital of Jining Medical University, Jining, Shandong, China.

Graphical Abstract

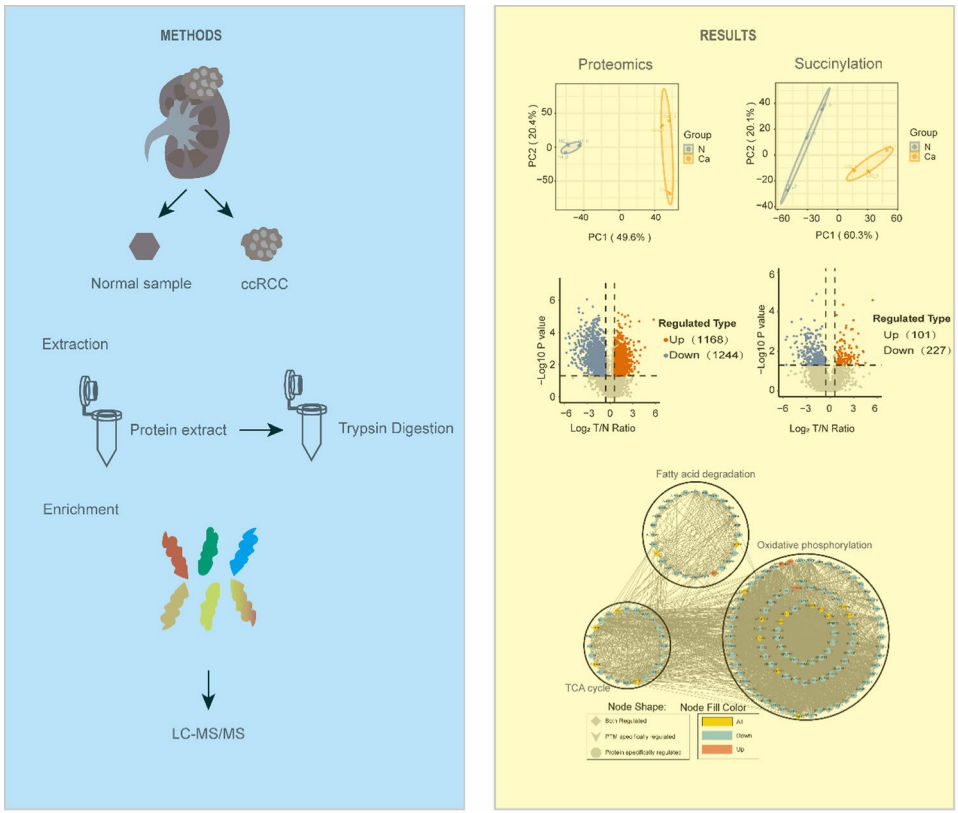

Keywords Clear cell renal cell carcinoma · Succinylation modification · Energy metabolism · Mitochondria

Abbreviations

BP	Biological process
CC	Cellular component
CHO	Cholesterol
COG	Cluster of orthologous
DDA	Data-dependent acquisition
DEPs	Differentially expressed proteins
FC	Fold change
FFA	Free fatty acid
FDR	False discovery fate
GO	Gene ontology
HADHA	Trifunctional enzyme subunit alpha
IDH2	Isocitrate dehydrogenase 2
KEGG	Kyoto encyclopedia of genes and genomes
K-Suss	Lysine succinylation
LC–MS/MS	Liquid chromatography mass spectrometry
LV	Left ventricle
LVEF	Left ventricle ejection fraction
LVFS	Left ventricle fractional shortening
MF	Molecular function
PASEF	Parallel accumulation serial fragmentation

PPI	Protein–protein interaction
PTM	Posttranslational modification
TCA cycle	Tricarboxylic acid cycle
TG	Triglyceride

1 Introduction

Renal cell carcinoma (RCC) is one of the top ten most prevalent malignancies worldwide, with an estimated 434,840 incident cases worldwide in 2022 [1]. Clear cell RCC (ccRCC) represents the most pervasive histological subtype [2]. To date, metastatic treatment options have been limited [3]. Metabolic deregulation and reprogramming of energetic metabolism is a crucial characteristic of ccRCC [4–7]. In particular the metabolic flux through glycolysis is partitioned [8, 9], and mitochondrial bioenergetics and Oxidative phosphorylation are impaired, as well as lipid metabolism [10–14]. In this scenario it has been shown that succinylation is an important regulator of cell metabolism and regulates many biological characteristics of renal cancer. These findings should be referenced and discussed.

Post-translational modification (PTM) is a critical regulatory mechanism that increases proteome diversity through chemical modifications at specific amino acid residues [15]. Succinylation is a distinct type of protein modification mediated by succinyl-CoA, capable of regulating protein stability and function [16]. Recently, Lysine succinylation has been linked to various pathological disorders by transferring a succinyl group to protein residue through either enzymatic or non-enzymatic processes [17, 18].

Given the critical importance of succinylation modifications and the existing research gaps in ccRCC, we conducted succinylation omics studies in ccRCC. This effort created a proteome atlas and an overview of succinylation PTM changes, comprehensively depicting the global proteome and succinylation modifications in ccRCC. Our analysis revealed a significant decrease in succinylation levels in ccRCC. Specifically, quantitative PTM omics identified 4801 succinylation-modified sites across 1274 proteins, with 434 sites in 328 proteins showing notable changes in ccRCC ($FC > 1.5$ or $p < 0.05$). Notably, some of these differentially succinylated sites were found on crucial proteins related to energy metabolism, indicating that succinylation modifications at these critical sites may significantly influence ccRCC progression. These findings pave the way for developing new therapeutic strategies for ccRCC.

2 Methods

2.1 Histological examination

The Declaration of Helsinki guidelines were followed during the investigation. This study was approved by the Ethics Committee of Affiliated Hospital of Jining Medical University (approval number: 2021-09-C016), and informed consent was obtained from all patients. 6 pathological specimens were collected from 3 ccRCC patients who underwent complete kidney removal at the Urology Department, Affiliated Hospital of Jining Medical University. A tumor-free area (3 cm beyond the tumor tissue) was selected for each patient as an internal control [19]. Tissue sections were hydrated using graded alcohol solutions after dewaxing in xylene [20]. Images were captured at 200× magnification using a fluorescent microscope (OLYMPUS DP72, Japan).

2.2 Transmission electron microscopy

The specimen was divided into 1 mm2 sample blocks with a sharp blade, fixed with 2.5% glutaraldehyde, and was fixed overnight at 4℃ away from light. After being fixed with 1% osmic acid at room temperature for one h, the tissue was immersed in 30% ethanol, 50% ethanol, 70% ethanol, 80% acetone, 90% acetone, and 30% ethanol, respectively, 95% acetone, 15 min each time; Samples were immersed in 100% acetone three times for 10 min each, followed by permeation and embedding in an epoxy resin. Using an ultra-thin microtome, cut the sample into slices of 300 μm × 300 μm with a thickness of 70 nm [21]. After dyeing with two drops of uranyl acetate on the copper mesh, staining it for 30 min

away from light, and leaving it to dry were observed under a Talos L120C (Thermo Scientific, USA) transmission electron microscope.

2.3 Western blot (WB)

Proteins extracted from frozen ccRCC and paracancer tissues were separated by SDS-PAGE and transferred to polyvinylidene difluoride membranes (0.45 μm). The membranes were then blocked with 5% nonfat milk for 1 h. Following this, the membranes were incubated with the primary antibody overnight at 4 °C, then with the secondary antibody at room temperature for 1 h, and detected using an enhanced chemiluminescence (ECL) system (Tanon5200, China) [22]. The antibodies used included anti-succinylated lysine (PTM419 1:1000; PTM Biolab), mouse IgG (H + L) secondary antibody (Pierce31430 1:1000; Thermo).

2.4 LC–MS/MS

Tryptic peptides were dissolved in solvent A and loaded onto a homemade reversed-phase column. The mobile phase included solvent A (0.1% formic acid, 2% acetonitrile in water) and solvent B (0.1% formic acid in acetonitrile). Peptide separation was performed using the following gradient: 0–18 min at 6–22% B; 18–22 min at 22–30% B; 22–26 min at 30–80% B; and 26–30 min at 80% B, all at a constant flow rate of 450 nL/min on a NanoElute UHPLC system (Bruker Daltonics). The peptides were analyzed on a timsTOF Pro mass spectrometry system, with an electrospray voltage of 1.65 kV. Precursors and fragments were analyzed using a TOF detector. The timsTOF Pro operated in data-independent parallel accumulation serial fragmentation (dia-PASEF) mode, with full MS scans set between 100–1700 m/z (MS/MS scan range), and eight PASEF (MS/MS mode) scans were acquired per cycle. The MS/MS scan range was set from 425–1025 m/z, and the isolation window was configured to 25 m/z [23].

2.5 Pan antibody-based succinylation PTM enrichment

To enrich the modified peptides, tryptic peptides in NETN buffer (which contains 100 mM NaCl, one mM EDTA, 50 mM Tris–HCl, 0.5% NP-40, pH 8.0) were incubated overnight at 4 °C with pre-washed antibody beads (Lot PTM402, PTM Bio) while gently shaking. The beads were washed four times with NETN buffer and twice with water. Bound peptides were eluted with 0.1% trifluoroacetic acid. The eluted fractions were combined and vacuum-dried. The resulting peptides were desalted for LC–MS/MS analysis using C18 ZipTips (Millipore), according to the manufacturer's instructions [23].

2.6 Data Search

DIA data were processed with Spectronaut (v.18). Tandem mass spectra were searched against the Homo_sapiens_9606_SP_20231220.fasta database (20,429 entries), concatenated with a reverse decoy database. Trypsin/P was used as the cleavage enzyme, permitting up to four missed cleavages. Carbamidomethylation on Cys was set as a fixed modification, while acetylation on the protein N-terminal, oxidation on Met, and succinylation on Lys were treated as variable modifications. The false discovery rate (FDR) of protein, peptide, and PSM was adjusted to < 1% [24].

2.7 Data analysis

The fold change (FC) was calculated as the ratio of the mean relative quantitative values of modified sites in the Tumor (T) group to the Control (C) group. An FC > 1.5 or < 1/1.5 threshold was used to identify differentially modified sites, indicating upregulated and downregulated proteins/sites. A student's t-test was performed on log2-transformed values with a p-value of less than 0.05, considered statistically significant.

2.8 Bioinformatics analysis

The proteome was annotated with gene ontology (GO) terms using the UniProt-GOA database. Proteins were classified by their roles in biological processes (BPs), cellular components (CCs), and molecular functions (MFs). Subcellular localization was predicted with Wolfpsort software. Based on motif-x, the MOMO software was used to generate sequence models around each modified site in protein sequences. It considered a sequence significant if it had more than 20 peptide segments and met the statistical p-value criteria. KEGG pathway analysis was performed using the DAVID database. The protein–protein interaction (PPI) network for Kbhb-modified proteins was constructed with the STRING database (v11) and visualized using Cytoscape (v.3.7.2).

2.9 Statistical analysis

Proteomic and succinylation modification analyses were performed on three samples from each group. Experiment reproducibility was evaluated using relative standard deviation, principal component analysis, and Pearson's correlation coefficient. Quantitative values are reported as mean ± SD for physiological data, and an independent Student's t-test was used to compare the Tumor and Control groups with SPSS 26.0 software. Statistical significance was set at $p < 0.05$. All graphs were generated using GraphPad Prism 8 software.

2.10 Ethics approval

This study was approved by the Ethics Committee of the Affiliated Hospital of Jining Medical University (approval number: 2021-09-C016). All procedures were carried out in strict accordance with the 1964 Declaration of Helsinki guidelines. All patients involved in this study provided informed consent before the study.

3 Results

3.1 Morphological phenotypical features in ccRCC

To investigate the pathogenesis of ccRCC, we first looked at the gross markers after radical nephrectomy. It is found that renal clear cell carcinoma is primarily located in the renal parenchyma, and there is often envelope formation between the tumor and surrounding normal renal tissue. The tumor section is yellowish-white, and the center has

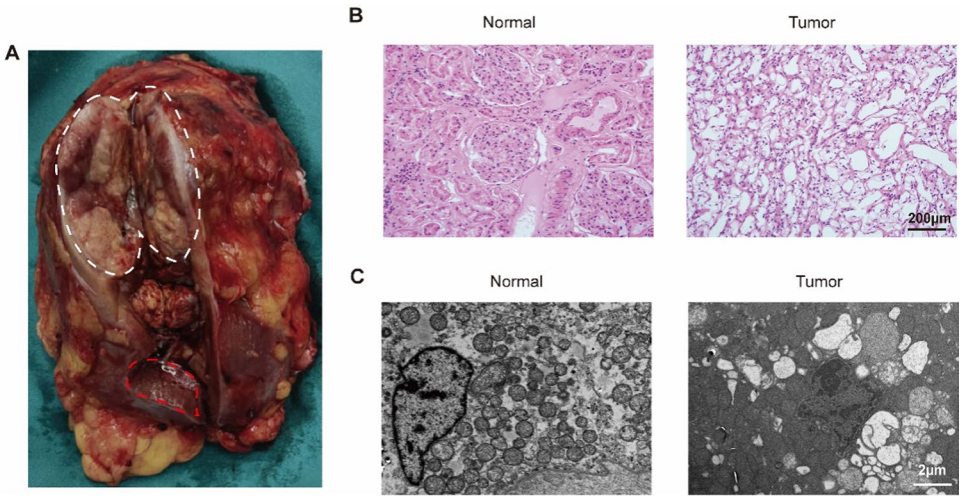

Fig. 1 Morphological analysis of ccRCC. **A** Postoperative specimen of renal carcinoma (The white dashed lines represent cancerous tissue, and the red dashed lines represent adjacent normal tissue). **B** HE staining of normal and ccRCC tissues. **C** Mitochondrial ultrastructures in each group under transmission electron microscope

Fig. 2 Whole proteome analysis of normal and ccRCC samples. **A** flowchart for the identification of omics in samples from normal and ccRCC ▶ samples. **B** Volcano plot of differential protein quantify for proteomics. Red represents upregulated proteins, and blue represents downregulated proteins. **C** Subcellular structure diagram of differential proteins. **D** GO analysis results of differential proteins (blue: biological process; yellow: cellular component; green: molecular function). **E** Top enriched items for KEGG pathway. **F** COG/KOG pathway of differential proteins (red: cellular processes and signaling, green: information storage and processing, blue: metabolism, yellow: poorly characterized). GO: gene ontology; KEGG: Kyoto Encylopedia of Genes and Genomes; COG/KOG: clusters of orthologous groups/eukaryotic ortholog groups

hemorrhagic necrosis, calcification, or jelly-like material. The larger the cancer, the more pronounced the necrosis is (Fig. 1A). In the HE-stained section, ccRCC can appear as a small nucleus with large volume, polygonal edges, and many lipid vacuoles in the cytoplasm (Fig. 1B). Given that mitochondria are essential for energy metabolism, we focused on the changes occurring in mitochondria in ccRCC. Transmission electron microscopy showed that although mitochondria were widely distributed, the ridge morphology was disordered in ccRCC ((Fig. 1C).

3.2 Quantification and identification of the global proteome were conducted using data-dependent acquisition (DDA) proteomics in ccRCC

To identify proteins associated with ccRCC, we conducted high-throughput proteomics analysis on tissue samples. A total of 8224 proteins were quantified in the tissues, resulting in 2412 differentially expressed proteins (DEPs) defined by a truncation value of 1.5-fold and a significance level of $p < 0.05$. Among these DEPs, 1168 proteins were upregulated, while 1244 were downregulated in ccRCC (Fig. 2B). Supplementary Data S1 details the DEPs, encompassing protein names, molecular weights, subcellular locations, and primary functions.

To understand the proteomic changes in ccRCC, differentially expressed proteins (DEPs) were classified according to their subcellular localization, biological processes (BPs), cellular components (CCs), and molecular functions (MFs). The results show that the most significant proportion (37.22%) was found in the mitochondria (Fig. 2C). GO analysis indicated that the proteins were predominantly associated with metabolic processes. At the same time, the CC category included terms such as intracellular, cytoplasm, and organelle, and most proteins fell under protein binding in the MF classification (Fig. 2D). Additionally, KEGG analysis highlighted proteins with significant differential enrichment, transport, and catabolism notably represented in the pathways for these differential proteins (Fig. 2E). COG analysis further indicated that many DEPs are involved in energy production and conversion (157 out of 488) (Fig. 2F).

3.3 Quantitative analysis of differentially succinylation modified proteins in ccRCC

Through Western blot analysis, this study examined lysine succinylation in ccRCC and normal tissues. The findings indicated that lysine succinylation was the most significantly reduced post-translational modification (PTM) in ccRCC (Fig. 3A), implying that succinylation levels are markedly inhibited in this cancer type. Using a 1.5-fold cutoff, we identified 132 sites in 101 upregulated proteins, while 302 sites in 227 were downregulated in ccRCC (Fig. 3B). Additionally, we assessed the subcellular localization of these proteins, revealing that a significant percentage were found in mitochondria (37.89%), suggesting that this organelle may be the primary site of succinylation (Fig. 3C). Supplementary Data S2 provides a detailed description.

3.4 Functional enrichment analysis of differentially succinylation modified proteins in ccRCC

We performed functional enrichment analysis to explore further the types of proteins preferentially modified by succinylation. The results showed cellular metabolic processes significantly enriched downregulated succinylation-modified proteins (Fig. 4A). Additionally, KEGG pathway enrichment analysis indicated that these downregulated proteins are linked to pathways related to carbohydrate metabolism, amino acid metabolism, and lipid metabolism (Fig. 4B). COG analysis also highlighted that a considerable proportion of the differentially expressed proteins (DEPs) are involved in energy production, conversion, lipid transport, and metabolism (Fig. 4C).

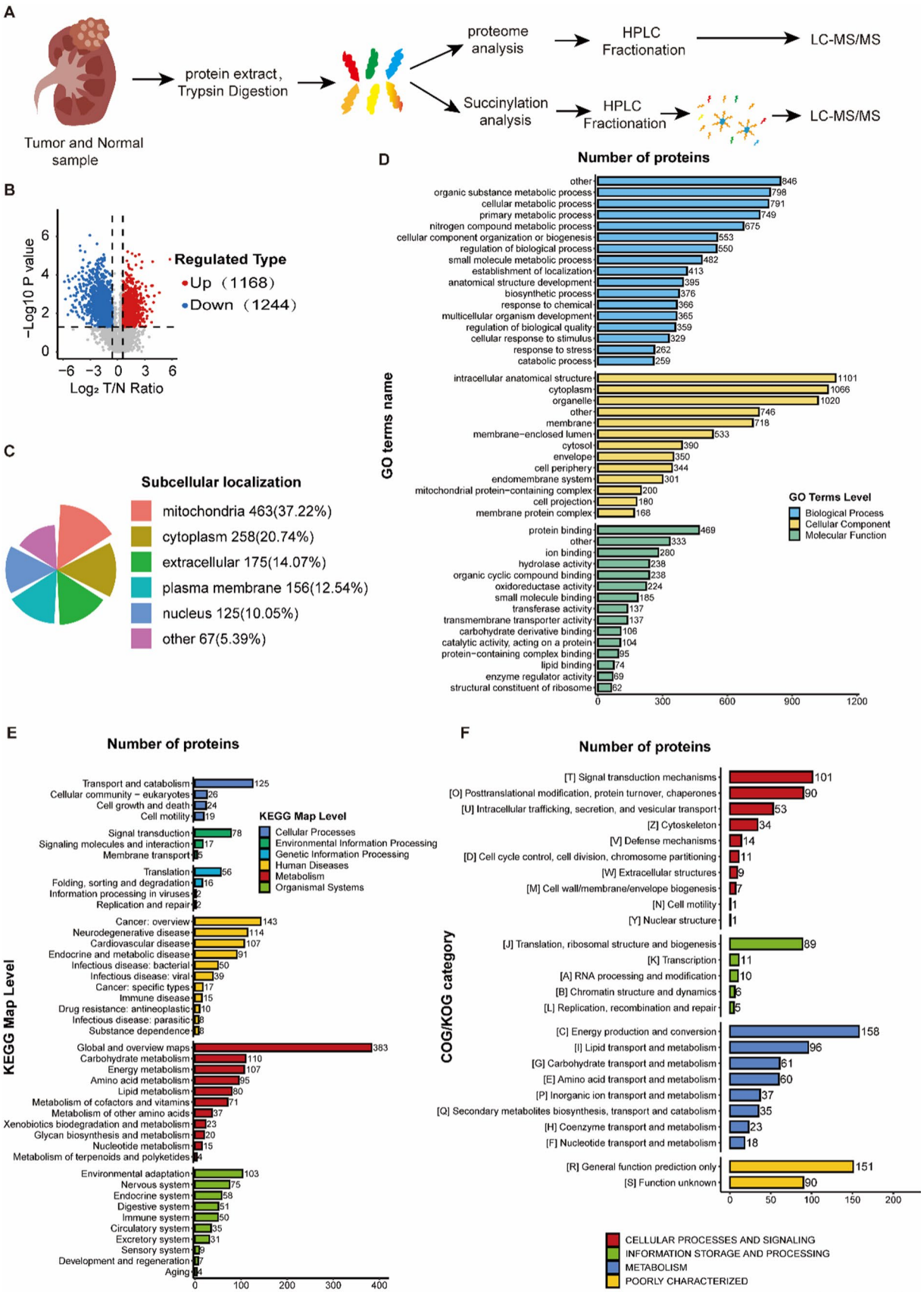
A
Tumor and Normal sample
protein extract, Trypsin Digestion
proteome analysis
HPLC Fractionation
LC-MS/MS
Succinylation analysis
HPLC Fractionation
LC-MS/MS
B
−Log10 P value
Log₂ T/N Ratio
Regulated Type
Up (1168)
Down (1244)
C
Subcellular localization
mitochondria 463(37.22%)
cytoplasm 258(20.74%)
extracellular 175(14.07%)
plasma membrane 156(12.54%)
nucleus 125(10.05%)
other 67(5.39%)
D
Number of proteins
GO terms name
other 846
organic substance metabolic process 798
cellular metabolic process 791
primary metabolic process 749
nitrogen compound metabolic process 675
cellular component organization or biogenesis 553
regulation of biological process 550
small molecule metabolic process 482
establishment of localization 413
anatomical structure development 395
biosynthetic process 376
response to chemical 366
multicellular organism development 365
regulation of biological quality 359
cellular response to stimulus 329
response to stress 262
catabolic process 259
intracellular anatomical structure 1101
cytoplasm 1066
organelle 1020
other 746
membrane 718
membrane−enclosed lumen 533
cytosol 390
envelope 350
cell periphery 344
endomembrane system 301
mitochondrial protein−containing complex 200
cell projection 180
membrane protein complex 168
protein binding 469
other 333
ion binding 280
hydrolase activity 238
organic cyclic compound binding 238
oxidoreductase activity 224
small molecule binding 185
transferase activity 137
transmembrane transporter activity 137
carbohydrate derivative binding 106
catalytic activity, acting on a protein 104
protein−containing complex binding 95
lipid binding 74
enzyme regulator activity 69
structural constituent of ribosome 62
GO Terms Level
Biological Process
Cellular Component
Molecular Function
E
Number of proteins
KEGG Map Level
Transport and catabolism 125
Cellular community − eukaryotes 26
Cell growth and death 24
Cell motility 19
Signal transduction 78
Signaling molecules and interaction 17
Membrane transport 15
Translation 56
Folding, sorting and degradation 16
Information processing in viruses 2
Replication and repair 2
Cancer: overview 143
Neurodegenerative disease 114
Cardiovascular disease 107
Endocrine and metabolic disease 91
Infectious disease: bacterial 50
Infectious disease: viral 39
Cancer: specific types 17
Immune disease 15
Drug resistance: antineoplastic 10
Infectious disease: parasitic 8
Substance dependence 8
Global and overview maps 383
Carbohydrate metabolism 110
Energy metabolism 107
Amino acid metabolism 95
Lipid metabolism 80
Metabolism of cofactors and vitamins 71
Metabolism of other amino acids 37
Xenobiotics biodegradation and metabolism 23
Glycan biosynthesis and metabolism 20
Nucleotide metabolism 15
Metabolism of terpenoids and polyketides 4
Environmental adaptation 103
Nervous system 75
Endocrine system 58
Digestive system 51
Immune system 50
Circulatory system 35
Excretory system 31
Sensory system 9
Development and regeneration 7
Aging 4
Cellular Processes
Environmental Information Processing
Genetic Information Processing
Human Diseases
Metabolism
Organismal Systems
F
Number of proteins
COG/KOG category
[T] Signal transduction mechanisms 101
[O] Posttranslational modification, protein turnover, chaperones 90
[U] Intracellular trafficking, secretion, and vesicular transport 53
[Z] Cytoskeleton 34
[V] Defense mechanisms 14
[D] Cell cycle control, cell division, chromosome partitioning 11
[W] Extracellular structures 9
[M] Cell wall/membrane/envelope biogenesis 7
[N] Cell motility 1
[Y] Nuclear structure 1
[J] Translation, ribosomal structure and biogenesis 89
[K] Transcription 11
[A] RNA processing and modification 10
[B] Chromatin structure and dynamics 6
[L] Replication, recombination and repair 5
[C] Energy production and conversion 158
[I] Lipid transport and metabolism 96
[G] Carbohydrate transport and metabolism 61
[E] Amino acid transport and metabolism 60
[P] Inorganic ion transport and metabolism 37
[Q] Secondary metabolites biosynthesis, transport and catabolism 35
[H] Coenzyme transport and metabolism 23
[F] Nucleotide transport and metabolism 18
[R] General function prediction only 151
[S] Function unknown 90
CELLULAR PROCESSES AND SIGNALING
INFORMATION STORAGE AND PROCESSING
METABOLISM
POORLY CHARACTERIZED

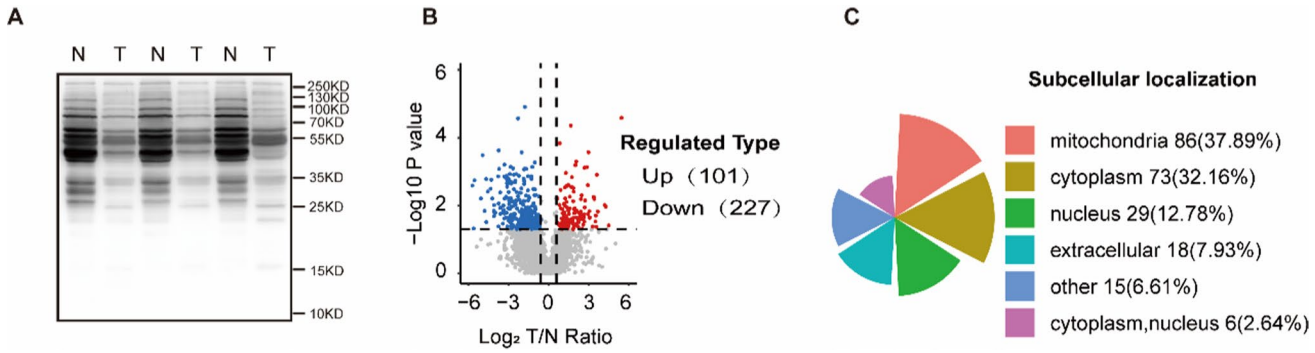

Fig. 3 Characteristics of succinylation modified proteins in ccRCC. **A** The level of lysine succinylation was examined through Western blot in normal and ccRCC tissues. **B** Volcano plot of significant identified sites. (FC > 1.5 or < 1/ 1.5). **C** Subcellular location of differential succinylation modified proteins

3.5 Quantification and identification of succinylation sites in ccRCC

Our current study found 512 proteins (40.19%, 512 out of 1274) had a single succinylation site (Fig. 5A). Notably, several specific proteins showed significant succinylation modifications (Fig. 5B), with many of them serving as regulators of energy metabolism. For instance, albumin has approximately seven binding sites, while trifunctional enzyme subunit alpha (HADHA) exhibited 44 succinylation sites.

Furthermore, we utilized MoMo software to analyze the flanking sequences extending from − 10 to + 10 around the succinylation modification site. The results indicated that glycine (G), valine (V), and tyrosine (Y) were most frequently found at the + 1 position, while alanine (A), aspartic acid (D), and valine (V) were predominant at the − 1 position surrounding the lysine succinylation sites (Fig. 5C).

3.6 Analysis of the PPI network between the global proteome and succinylation-modified proteome in ccRCC

To examine the relationship between the proteome and succinylation-modified proteins, we conducted a protein–protein interaction (PPI) network analysis to identify critical nodes and significant biological processes associated with differentially expressed proteins (DEPs) and succinylation-modified proteins (Fig. 6B). KEGG enrichment analysis and categorization revealed that downregulated succinylation-modified proteins were notably enriched in pathways such as mitochondrial oxidative phosphorylation, fatty acid degradation, and the TCA cycle (Tables 1, 2, 3). We further analyzed the interaction network of differential and succinylation-modified proteins related to these three pathways using the STRING v.11.0 database.

In the PPI network analysis, we identified seven proteins with significantly downregulated succinylation modifications associated with oxidative phosphorylation, thirteen proteins related to fatty acid degradation, and eight proteins involved in the TCA cycle (Fig. 6C). These results indicate that the succinylation modifications of these essential enzymes play a crucial role in the energy regulatory mechanisms during the progression of ccRCC.

4 Discussion

The American Cancer Society projects that by the end of 2023, around 81,800 new cases of renal cell carcinoma (RCC) will be diagnosed in the United States, with more than 14,890 deaths resulting from the disease [25]. The most common subtype of RCC is ccRCC, which accounts for approximately 75% of all cases [26]. The propensity of detecting ccRCC at a later stage greatly diminishes disease-specific survival rates [27]. In ccRCC, the tricarboxylic acid cycle (TCA cycle), glucose metabolism, and fatty acid metabolism show alterations, indicating a reprogramming of these metabolic pathways [6, 28].

Post-translational modifications (PTMs) are vital in regulating protein functions and have been associated with ccRCC [29]. Lysine succinylation is an emerging type of PTM where a succinyl group attaches to a lysine residue, resulting in substantial chemical and structural alterations to the affected protein [30]. However, in the field of ccRCC research, the

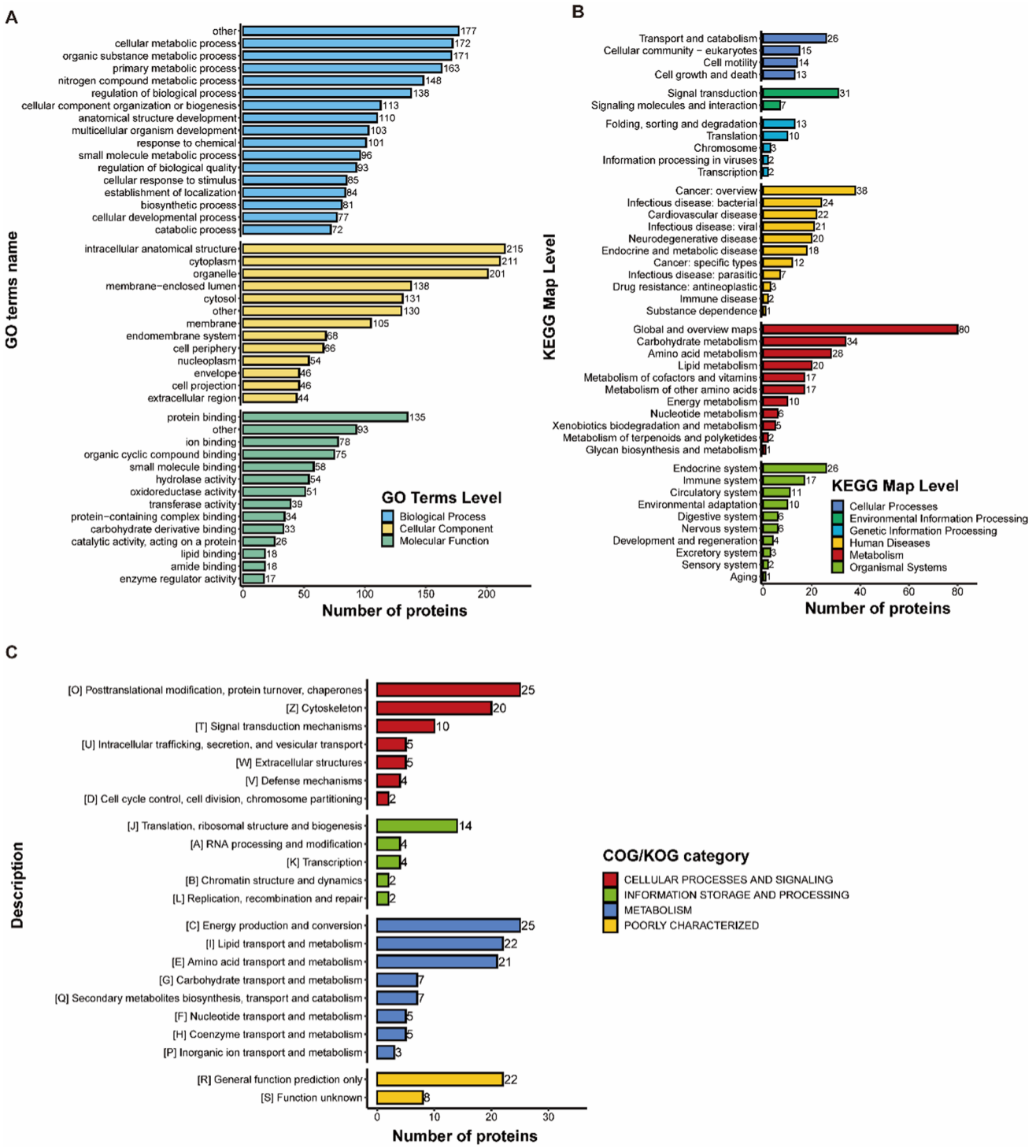

Fig. 4 Functional Enrichment Analysis of Differentially Succinylation Modified Proteins in ccRCC. **A** GO classification of differential succinylation modified proteins (blue: biological process; yellow: cellular component; green: molecular function). **B** Top enriched items for KEGG pathway. **C** COG/KOG pathway of differential proteins (red: cellular processes and signaling, green: information storage and processing, blue: metabolism, yellow: poorly characterized)

precise impacts of Lysine succinylation have yet to be well described. In this study, we conducted a high-throughput quantitative proteomics analysis, identifying 434 significantly differentially modified sites across 328 proteins in ccRCC. Our findings revealed that many succinylation-modified sites on crucial enzymes were related to energy metabolism.

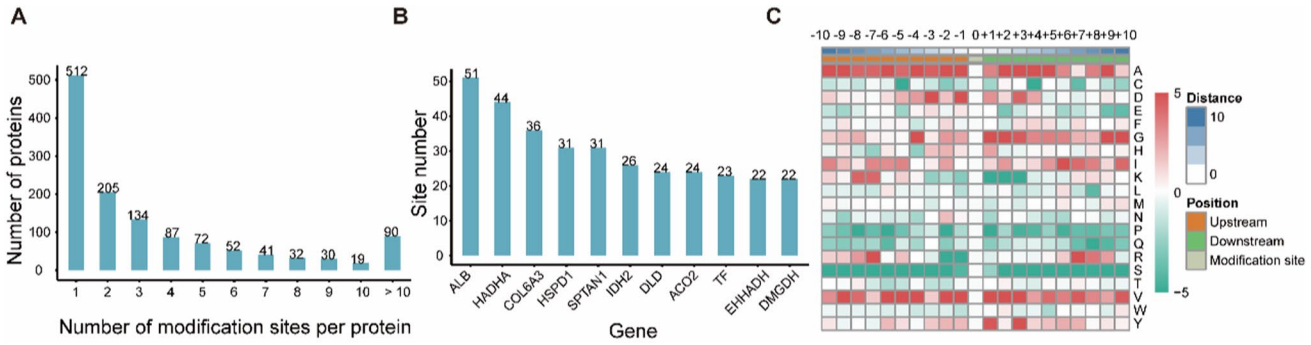

Fig. 5 Characteristics of succinylation-modified sites in ccRCC. **A** Distribution of the number of the succinylation-modified sites per protein. **B** Statistical map of proteins with > 10 succinylation-modified sites. **C** A heat map of the ± 10 amino acid compositional frequencies surrounding the succinylation-modified sites

In this study, we noted significant phenotypic changes linked to ccRCC. These changes included Tumor morphology, histology, and microscopic mitochondrial morphology (Fig. 1); notably, our TEM results indicate that the mitochondrial cristae were flattened and absent in ccRCC, suggesting a dysfunction in energy metabolism in this condition [31].

Previously, succinylation was associated with the initiation and progression of cancer [32]. Our present study analyzed lysine succinylation in the ccRCC and adjacent normal tissues based on WB analysis. The levels of lysine succinylation proteins were significantly lower in ccRCC, highlighting the critical role of succinylation in this disease. To thoroughly examine the changes in global succinylation modification in ccRCC, we used quantitative proteomics and succinylation PTM omics on ccRCC and adjacent normal tissues. Our quantitative proteomics analysis identified 8224 proteins, with 2412 showing significant differential expression between ccRCC and adjacent normal tissues. Notably, 32.4% of the succinylation sites showed substantial changes that were mirrored by corresponding shifts at the protein level, indicating that succinylation modification is crucial in the progression of ccRCC.

Mitochondria are particularly abundant in the kidney, which removes waste from the blood and regulates fluid and electrolyte balance [33]. Mitochondria provide the energy to drive these essential functions and play a crucial role in protein PTMs by supplying acyl-CoA donors necessary for various acylation processes, including succinylation [34, 35]. Our study revealed that 37.9% of succinylation-modified proteins were located in the mitochondria. This suggests that mitochondrial proteins undergo substantial alterations in succinylation modification, indicating that mitochondria are the primary sites for succinylation in ccRCC.

Similar patterns were noted for succinylation in RCC [36], numerous energy metabolism pathways, such as fatty acid β-oxidation, the TCA cycle, and oxidative phosphorylation, showed significant enrichment in succinylation. Key enzymes involved in these processes possess at least one succinylation site. Albumin, primarily functioning as a fatty acid-binding protein in extracellular fluids, plays a crucial role in this context and exhibited downregulation of succinylation modification in ccRCC. Plasma albumin has approximately seven binding sites for fatty acids with varying degrees of moderate to high affinity, indicating that succinylation modifications may influence its activity and function [37]. The trifunctional enzyme subunit alpha (HADHA), an enzyme involved in mitochondrial β-oxidation [38], displayed 44 succinylation sites and reduced succinylation modification across multiple sites in ccRCC. The finding indicates that succinylation modification may impact βHB production. IDH2, a mitochondrial protein that controls TCA cycle flux [39, 40], contains 26 regulated sites in ccRCC. This phenomenon suggests that succinylation modification may influence mitochondrial respiration and energy production.

In this study, we presented a global proteomic profile and a detailed succinylation modification landscape in ccRCC. However, there were some limitations in this study. Our exploration was limited to three ccRCC patients, which is a relatively small sample size. This limits the generalizability of the findings and may not fully represent the heterogeneity of ccRCC. Our future directions will focus on functional experiments using diverse tumor systems (e.g., PDX, organoids) to confirm the biological relevance of these modifications in ccRCC progression and expanding clinical validation through larger cohort studies.

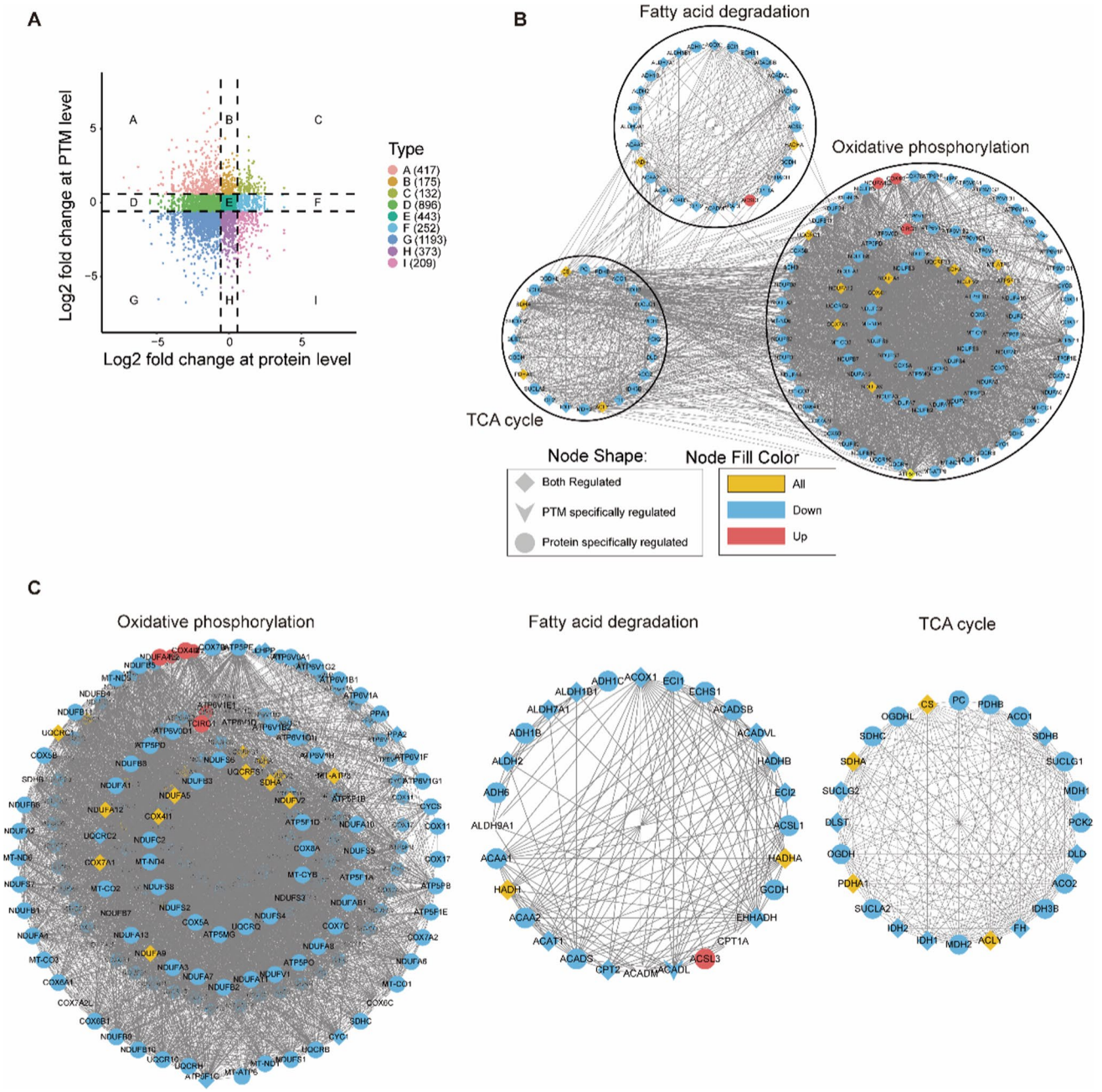

Fig. 6 Protein–protein interactions network between global proteome and succinylation modified proteome in ccRCC. **A** Nine-quadrant diagram of the correlation of log2 (FC) of DEPs and differentially succinylation modified proteome in ccRCC (log FC > 1.5; p-value < 0.05). Quadrant-A (QA) were those proteins that were upregulated in the proteome, whereas declined in succinylation modified proteome; Quadrant-B (QB) were proteins upregulated in the proteome, whereas they were unaltered in succinylation modified proteome; Quadrant-C (QC) were proteins that were upregulated in proteome and succinylation modified proteome; Quadrant-D (QD) were proteins that were unaltered in the proteome, whereas downregulated in succinylation modified proteome; Quadrant-E (QE) were proteins unaltered in proteome and succinylation modified proteome; Quadrant-F (QF) were proteins that were unaltered in proteome, but increased in succinylation modified proteome; Quadrant-G (QG) were proteins downregulated in proteome and succinylation modified proteome, Quadrant-H (QH) were proteins downregulated in proteome, but were unaltered in succinylation modified proteome; Quadrant-I (QI) were proteins downregulated in proteome, but were upregulated in succinylation modified proteome. **B** The PPI network of proteome and succinylation modified proteome. **C** The PPI network of proteome and succinylation modified proteome of oxidative phosphorylation, fatty acid degradation, and TCA cycle. The circle represents specifically differentially expressed protein without differentially modified sites, the arrow represents specifically differentially modified site without change in proteome, and the diamond represents both differentially expression in proteome and modification. Blue represents downregulation in proteome or succinylation modification; Red represents upregulation in proteome or succinylation modification; Yellow represents downregulation and upregulation in proteome or succinylation modification

Table 1 Downregulated succinylation-modified sites of oxidative phosphorylation pathway

Protein description	Gene name	Amino acid	Sites	T/N ratio	T/N p value
Cytochrome c oxidase subunit 7A-related protein	COX7A2L	K	65	0.354830581	0.027976693
Cytochrome c1, heme protein	CYC1	K	318	0.409357305	0.049626339
Cytochrome b-c1 complex subunit 2	UQCRC2	K	430	0.386269102	0.020730414
ATP synthase subunit gamma	ATP5F1C	K	83	0.474326096	0.004983229
Phospholysine phosphohistidine	LHPP	K	183	0.13948268	0.040877516
Inorganic pyrophosphatase	PPA2	K	259	0.073496015	0.041861319
NADH dehydrogenase ubiquinone subcomplex subunit 12	NDUFA12	K	101	0.52183376	0.039854516

T: tumor tissue; N: normal tissue

Table 2 Downregulated succinylation-modified sites of fatty acid degradation

Protein description	Gene name	Amino acid	Sites	T/N ratio	T/N p value
Enoyl-CoA delta isomerase 2	ECI2	K	359	0.111008204	0.016633216
Aldehyde dehydrogenase	ALDH2	K	368	0.157725741	0.023937248
Aldehyde dehydrogenase	ALDH2	K	378	0.083652464	0.011413795
Medium-chain specific acyl-CoA dehydrogenase	ACADM	K	178	0.217341825	0.015157404
Carnitine O-palmitoyltransferase 2	CPT2	K	510	0.138311724	0.002013986
Acetyl-CoA acetyltransferase	ACAT1	K	40	0.262937874	0.029621856
Acetyl-CoA acetyltransferase	ACAT1	K	202	0.225532487	0.049509715
Long-chain specific acyl-CoA dehydrogenase	ACADL	K	81	0.170725481	0.017850459
Aldehyde dehydrogenase X	ALDH1B1	K	379	0.305408054	0.01143473
4-trimethylaminobutyraldehyde dehydrogenase	ALDH9A1	K	303	0.400424254	0.001394885
Alpha-aminoadipic semialdehyde dehydrogenase	ALDH7A1	K	390	0.142444976	0.007864483
Very long-chain specific acyl-CoA dehydrogenase	ACADVL	K	372	0.215976937	0.027974519
Trifunctional enzyme subunit beta	HADHB	K	201	0.249902055	0.032082659
Trifunctional enzyme subunit beta	HADHB	K	277	0.162527802	0.0012468
Trifunctional enzyme subunit beta	HADHB	K	291	0.165526625	0.001234041
Trifunctional enzyme subunit beta	HADHB	K	408	0.31127091	0.031230219
Peroxisomal bifunctional enzyme	EHHADH	K	33	0.242246688	0.042697811
Peroxisomal bifunctional enzyme	EHHADH	K	350	0.351061129	0.021916607
Peroxisomal bifunctional enzyme	EHHADH	K	535	0.184584212	0.007578185
Peroxisomal bifunctional enzyme	EHHADH	K	700	0.12479319	0.028234593
Peroxisomal acyl-coenzyme A oxidase 1	ACOX1	K	504	0.210436892	0.001343044

T: tumor tissue; N: normal tissue

Table 3 Downregulated succinylation-modified sites of TCA cycle

Protein description	Gene name	Amino acid	Sites	T/N ratio	T/N p value
Isocitrate dehydrogenase [NADP] cytoplasmic	IDH1	K	81	0.4841071	0.003377868
Fumarate hydratase	FH	K	94	0.240991184	0.033643018
Dihydrolipoyl dehydrogenase	DLD	K	346	0.558427511	0.030053221
Succinate dehydrogenase ubiquinone iron-sulfur subunit	SDHB	K	55	0.308788649	0.038614337
Succinate dehydrogenase ubiquinone iron-sulfur subunit	SDHB	K	123	0.289382278	0.045199231
Dihydrolipoyllysine-residue succinyltransferase component of 2-oxoglutarate dehydrogenase complex	DLST	K	277	0.375007165	0.026892354
Isocitrate dehydrogenase [NADP]	IDH2	K	69	0.166483962	0.021264644
ATP-citrate synthase	ACLY	K	978	0.132983225	0.002258625
Succinate–CoA ligase [GDP-forming] subunit beta	SUCLG2	K	47	0.399527064	0.014191232

T: tumor tissue; N: normal tissue

5 Conclusions

In conclusion, our extensive quantitative analysis of succinylation modifications in ccRCC offers new insights into its role, particularly in regulating proteins associated with energy metabolism. These findings pave the way for potential therapeutic strategies to target and reverse abnormal succinylation modifications in ccRCC treatment.

Acknowledgements This research was funded by Jining Key Project of Research and Development Program, Grant Number 2023YXNS116, 2023YXNS125; Talent program of Affiliated Hospital of Jining Medical University, Grant Number 2023-yxyc-005.

Author contributions Methodology, M.Z.; formal analysis, M.Z.; investigation, D.Y.; resources, D.Y.; writing—original draft preparation, D.Y.; supervision, M.Z.; project administration, M.Z.; funding acquisition, M.Z. All authors reviewed the manuscript.

Data availability Data is provided within the supplementary information files.

Declarations

Competing interests The authors declare no competing interests.

References

1. Rose TL, Kim WY. Renal cell carcinoma: a review. JAMA. 2024;332(12):1001–10.
2. Hsieh JJ, Purdue MP, Signoretti S, et al. Renal cell carcinoma. Nat Rev Dis Primers. 2017;3:17009.
3. Wettersten HI, Aboud OA, Lara PN Jr, Weiss RH. Metabolic reprogramming in clear cell renal cell carcinoma. Nat Rev Nephrol. 2017;13(7):410–9.
4. Hu J, Wang SG, Hou Y, et al. Multi-omic profiling of clear cell renal cell carcinoma identifies metabolic reprogramming associated with disease progression. Nat Genet. 2024;56(3):442–57.
5. di Meo NA, et al. The dark side of lipid metabolism in prostate and renal carcinoma: novel insights into molecular diagnostic and biomarker discovery. Expert Rev Mol Diagn. 2023;23:297–313.
6. Lucarelli G, et al. Metabolomic insights into pathophysiological mechanisms and biomarker discovery in clear cell renal cell carcinoma. Expert Rev Mol Diagn. 2019;19:397–407.
7. di Meo NA, et al. Renal cell carcinoma as a metabolic disease: an update on main pathways, potential biomarkers, and therapeutic targets. Int J Mol Sci. 2022;23:14360.

8. Lucarelli G. et al. Transcriptomic and proteo-metabolic determinants of the grading system in clear cell renal cell carcinoma. Urol Oncol S1078–1439(25)00065–00061.
9. Lucarelli G, et al. Metabolomic profile of glycolysis and the pentose phosphate pathway identifies the central role of glucose-6-phosphate dehydrogenase in clear cell-renal cell carcinoma. Oncotarget. 2015;6:13371–86.
10. Lucarelli G, et al. Integrated multi-omics characterization reveals a distinctive metabolic signature and the role of NDUFA4L2 in promoting angiogenesis, chemoresistance, and mitochondrial dysfunction in clear cell renal cell carcinoma. Aging (Albany NY). 2018;10:3957–85.
11. Bombelli S, et al. 36-kDa Annexin A3 isoform negatively modulates lipid storage in clear cell renal cell carcinoma cells. Am J Pathol. 2020;190:2317–26.
12. Bianchi C, et al. The glucose and lipid metabolism reprogramming is grade-dependent in clear cell renal cell carcinoma primary cultures and is targetable to modulate cell viability and proliferation. Oncotarget. 2017;8:113502–15.
13. Lucarelli G, et al. MUC1 tissue expression and its soluble form CA15-3 identify a clear cell renal cell carcinoma with distinct metabolic profile and poor clinical outcome. Int J Mol Sci. 2022;23:13968.
14. Milella M, et al. The role of MUC1 in renal cell carcinoma. Biomolecules. 2024;14:315.
15. Beltrao P, Bork P, Krogan NJ, van Noort V. Evolution and functional cross-talk of protein post-translational modifications. Mol Syst Biol. 2013;9:714.
16. Shen R, Ruan H, Lin S, et al. Lysine succinylation, the metabolic bridge between cancer and immunity. Genes Dis. 2023;10(6):2470–8.
17. Dai X, Zhou Y, Han F, Li J. Succinylation and redox status in cancer cells. Front Oncol. 2022;12:1081712.
18. Mu R, Ma Z, Lu C, et al. Role of succinylation modification in thyroid cancer and breast cancer. Am J Cancer Res. 2021;11(10):4683–99.
19. Eun JW, Yoon JH, Ahn HR, et al. Cancer-associated fibroblast-derived secreted phosphoprotein 1 contributes to resistance of hepatocellular carcinoma to sorafenib and lenvatinib. Cancer Commun. 2023;43(4):455–79.
20. Zhang T, Zhang X, Fei Y, et al. Gallic acid suppresses the progression of clear cell renal cell carcinoma through inducing autophagy via the PI3K/Akt/Atg16L1 signaling pathway. Int J Oncol. 2024;65(1):70.
21. Tizro P, Choi C, Khanlou N. Sample preparation for transmission electron microscopy. Methods Mol Biol. 2019;1897:417–24.
22. Wang S, et al. MT1G induces lipid droplet accumulation through modulation of H3K14 trimethylation accelerating clear cell renal cell carcinoma progression. Br J Cancer. 2024;131:641–54.
23. Yang X, et al. Proteomics and β-hydroxybutyrylation modification characterization in the hearts of naturally senescent mice. Mol Cell Proteomics. 2023;22: 100659.
24. Ding WJ, Li XH, Tang CM, et al. Quantification and proteomic characterization of β-hydroxybutyrylation modification in the hearts of AMPKα2 knockout mice. Mol Cell Proteomics. 2023;22(2): 100494.
25. Siegel RL, Miller KD, Wagle NS, Jemal A. Cancer statistics, 2023. CA Cancer J Clin. 2023;73(1):17–48.
26. Leibovich BC, Lohse CM, Cheville JC, et al. Predicting oncologic outcomes in renal cell carcinoma after surgery. Eur Urol. 2018;73(5):772–80.
27. Saeednejad Zanjani L, Madjd Z, Axcrona U, et al. Cytoplasmic expression of B7–H3 and membranous EpCAM expression are associated with higher grade and survival outcomes in patients with clear cell renal cell carcinoma. Ann Diagn Pathol. 2020;46: 151483.
28. Qi X, Li Q, Che X, Wang Q, Wu G. The uniqueness of clear cell renal cell carcinoma: summary of the process and abnormality of glucose metabolism and lipid metabolism in ccRCC. Front Oncol. 2021;11: 727778.
29. Santorelli L, Capitoli G, Chinello C, et al. In-depth mapping of the urinary N-glycoproteome: distinct signatures of ccRCC-related progression. Cancers. 2020;12(1):239.
30. Zhao G, Zhen J, Liu X, et al. Protein post-translational modification by lysine succinylation: biochemistry, biological implications, and therapeutic opportunities. Genes Dis. 2023;10(4):1242–62.
31. Xu W, Liu WR, Xu Y, et al. Hexokinase 3 dysfunction promotes tumorigenesis and immune escape by upregulating monocyte/macrophage infiltration into the clear cell renal cell carcinoma microenvironment. Int J Biol Sci. 2021;17(9):2205–22.
32. Lu W, Che X, Qu X, et al. Succinylation regulators promote clear cell renal cell carcinoma by immune regulation and RNA N6-methyladenosine methylation. Front Cell Dev Biol. 2021;9: 622198.
33. Wasada T, Kodama Y, Inoue K, Hisatomi A, Sako Y, Ibayashi H. Plasma somatostatin response in normal and gastrectomized subjects. Tohoku J Exp Med. 1986;150(2):181–8.
34. Goetzman ES, Zhang BB, Zhang Y, et al. Dietary dicarboxylic acids provide a non-storable alternative fat source that protects mice against obesity. J Clin Invest. 2024;134(12): e174186.
35. Tillander V, Arvidsson Nordström E, Reilly J, et al. Acyl-CoA thioesterase 9 (ACOT9) in mouse may provide a novel link between fatty acid and amino acid metabolism in mitochondria. Cell Mol Life Sci. 2014;71(5):933–48.
36. Zheng L, Zhu ZR, Sneh T, et al. Circulating succinate-modifying metabolites accurately classify and reflect the status of fumarate hydratase-deficient renal cell carcinoma. J Clin Invest. 2023;133(11): e165028.
37. van der Vusse GJ. Albumin as fatty acid transporter. Drug Metab Pharmacokinet. 2009;24(4):300–7.
38. Pan A, Sun XM, Huang FQ, et al. The mitochondrial β-oxidation enzyme HADHA restrains hepatic glucagon response by promoting β-hydroxybutyrate production. Nat Commun. 2022;13(1):386.
39. Wang H, Xiong Q, He G, et al. Hepatic IDH2 regulates glycolysis and gluconeogenesis. Metabolism. 2023;143: 155559.
40. Shigeta K, Hasegawa M, Hishiki T, et al. IDH2 stabilizes HIF-1α-induced metabolic reprogramming and promotes chemoresistance in urothelial cancer. EMBO J. 2023;42(4): e110620.